

# RSC Advances



This is an *Accepted Manuscript*, which has been through the Royal Society of Chemistry peer review process and has been accepted for publication.

*Accepted Manuscripts* are published online shortly after acceptance, before technical editing, formatting and proof reading. Using this free service, authors can make their results available to the community, in citable form, before we publish the edited article. This *Accepted Manuscript* will be replaced by the edited, formatted and paginated article as soon as this is available.

You can find more information about *Accepted Manuscripts* in the [Information for Authors](#).

Please note that technical editing may introduce minor changes to the text and/or graphics, which may alter content. The journal's standard [Terms & Conditions](#) and the [Ethical guidelines](#) still apply. In no event shall the Royal Society of Chemistry be held responsible for any errors or omissions in this *Accepted Manuscript* or any consequences arising from the use of any information it contains.

## ARTICLE

## Integration of plasmonic semiconductor with metal-organic framework: A case of Ag/AgCl@ZIF-8 with enhanced visible light photocatalytic activity

Cite this: DOI: 10.1039/x0xx00000x

Received 00th January 2012,  
Accepted 00th January 2012

DOI: 10.1039/x0xx00000x

www.rsc.org/

Shu-Tao Gao, Wei-Hua Liu, Ning-Zhao Shang, Cheng Feng, Qiu-Hua Wu, Zhi Wang, Chun Wang\*

*College of Science, Agricultural University of Hebei, Baoding 071001, China*

Efficient utilization of solar energy has received tremendous attention due to the increasing environmental and energy concerns. In this paper, a plasmonic photocatalyst integrated with metal-organic framework (MOF) material, Ag/AgCl@ZIF-8, was fabricated for the first time. The unique hetero-junction structure of Ag/AgCl@ZIF-8 greatly enhanced its photocatalytic activity. Selecting RhB as a model pollutant, 98% of RhB can be degraded after 16 min under solar radiation. The relationship between the photocatalytic activity and the structure of Ag/AgCl@ZIF-8 hybrid materials was discussed and the possible reaction mechanism was proposed. The high photocatalytic activity of the hybrid material under solar radiation revealed its great application potential in directly harvesting solar energy to solve the environmental pollution issues.

### Introduction

With increasing consumption of energy, dwindling fossil fuel supplies and growing environmental contaminations, finding alternative and sustainable energy sources has become one of the most important and challenging tasks. Solar energy from sunlight is widely believed to be the key to solving the problems of the environment and energy resource because of its clean, sustainable, abundant and economical characteristics.<sup>1</sup> To efficient harvest of solar energy, various kinds of photocatalysts have been explored for the applications in splitting water into hydrogen, photocatalytic degradation of organic pollutants, preparing dye sensitized solar cells and so on.<sup>2</sup> However, the quantum yield and solar energy conversion efficiency of these developed photocatalysts are still relatively low, which limits their practical applications in different fields. Therefore, it is still attractive to explore new photocatalysts with improved activities, acceptable stability and low cost, especially visible-light-responsive photocatalysts because sunlight is mostly composed of visible light.

Currently, metal-organic frameworks (MOFs) have received significant attention in recent years as a novel class of nanoporous materials mainly due to their tunable pore sizes, high specific surface areas, the possibility to functionalize, and designable framework structures modularly built from transition-metal clusters as nodes and organic ligands as struts. Due to their outstanding features, they have found potential

applications in gas storage,<sup>3-5</sup> chemical separation,<sup>6</sup> heterogeneous catalysis,<sup>7-10</sup> and optical,<sup>2, 11</sup> electronic,<sup>12-14</sup> and magnetic materials.<sup>15</sup> In contrast, research concerning the applications of MOFs in photocatalysis is still in their infancy,<sup>2</sup> such as MOF-5,<sup>16</sup> MIL-53(M)(M= Al, Cr, Fe),<sup>17</sup> MIL-88B(Fe)<sup>18</sup> and NTU-9<sup>19</sup> have already been demonstrated to have semiconductor properties and used as photocatalyst for the degradation of organic pollutants molecules. However, the photocatalytic performance of them is lower than that of inorganic semiconductors due to MOF's low efficiency in exciton generation and low charge mobility.

Heterostructures integrating MOFs with light-harvesting semiconductor materials might be an effective approach to obtain efficient photocatalyst. Zhan et al.<sup>11</sup> prepared metal oxide semiconductor@MOF core-shell heterostructures, which display distinct photoelectrochemical response to hole scavengers. Wee et al.<sup>20</sup> integrated ZnO with ZIF-8 by a spontaneous phase segregation of ZIF-8 in silver nitrate aqueous and the as-prepared ZnO@ZIF-8 was used as photocatalyst for degradation of methylene blue under UV light. More recently, Li et al.<sup>21</sup> prepared Cu<sub>3</sub>(BTC)<sub>2</sub>@TiO<sub>2</sub> core-shell structures and examined their photocatalytic performance by using CO<sub>2</sub> conversion as a model system. Despite recent progress, MOF-based visible-light responsive photocatalyst still remains untouched.

Ag/AgX, which exhibit high absorption in the visible region

due to the surface plasmon resonance (SPR) of silver nanoparticles, represents a class of highly efficient visible-light-driven photocatalyst.<sup>22,23</sup> However, some challenges and problems still exist for Ag/AgX photocatalyst, such as aggregation of the Ag/AgX particulates, the poor adsorptive property of Ag/AgX, the short lifetime of the photogenerated electron-hole pair, the low stability, and the limited visible-light response.

In this paper, to explore efficient visible-light responsive photocatalyst, plasmonic Ag/AgCl was integrated with zeolitic imidazolate framework 8 (ZIF-8) for the first time, in which Ag/AgCl nanoparticles to generate excitons and ZIF-8 structure to capture dye molecules. ZIF-8 was chosen as the metal-organic framework material because it has large specific surface area, reversible guest trapping and excellent thermal and chemical stability. Moreover, it is one of the few commercially available MOFs because of its great application potential in gas separation,<sup>24</sup> sensing<sup>25</sup> and catalysis.<sup>26</sup> The photocatalytic activity of the Ag/AgCl@ZIF-8 was investigated for the degradation of rhodamine-B (RhB). The results demonstrated that the as-prepared Ag/AgCl@ZIF-8 photocatalysts exhibit high activity and durability towards the decomposition of RhB under visible light irradiation. On the basis of the obtained findings, the Ag/AgCl@ZIF-8 photocatalyst was further tailored to directly harvest sunlight for the degradation of RhB.

## Experimental

### Chemicals

2-Methylimidazole (99%, MIm) and P25 were purchased from Aladdin Reagent Limited Company and used as received.  $\text{Zn}(\text{NO}_3)_2 \cdot 6\text{H}_2\text{O}$  (99%), rhodamine B, sodium chloride and silver nitrate were obtained from Chengxin Chemical Reagents Company (Baoding, China) and used without further purification. Methanol and ethanol were all provided by the Boaixin Co., Ltd. (Baoding, China)

### Characterizations

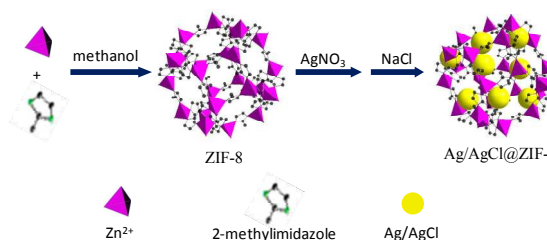
The size and morphology of the catalyst were observed by scanning electron microscopy (SEM) using a FEI Quanta 200F field emission electron microscope operated at 30 kV. The X-ray diffraction (XRD) patterns of the samples were recorded with a Rigaku D/max 2500 X-ray diffractometer using  $\text{Cu K}\alpha$  radiation (40 kV, 150 mA) in the range  $2\theta = 10^\circ\text{--}80^\circ$ . X-ray photoelectron spectroscopy (XPS) was performed with a PHI 1600 spectroscope using  $\text{Mg K}\alpha$  X-ray source for excitation. The diffuse reflectance spectra (DRS) were measured by a UV-vis spectrometer (UV-3600, Shimadzu) in the range of 300–800 nm.  $\text{BaSO}_4$  was used as the reflectance standard material. The Brunauer-Emmett-Teller (BET) surface area and porous structure were measured using an ASAP 2020 V3.01 H apparatus (Micromeritics Instrument Corp., USA). After the samples were degassed in vacuum at  $120^\circ\text{C}$  for 6 h, the nitrogen adsorption and desorption isotherms were measured at 77 K.

### Synthesis of ZIF-8 nanocrystals

ZIF-8 nanocrystals were prepared according to the previous synthesis protocol.<sup>27</sup> Typically, a solution of  $\text{Zn}(\text{NO}_3)_2 \cdot 6\text{H}_2\text{O}$  (2.348 g, 7.89 mmol) in 160 mL of methanol is rapidly poured into a solution of 2-methylimidazole (5.192 g, 63.24 mmol) in 160 mL of methanol under magnetic stirring. The mixture was stirred at room temperature for 2 h. The solid product was separated from the milky colloidal dispersion by centrifugation. After being washed with anhydrous ethanol and centrifugation three times, the white ZIF-8 product was dried in a vacuum at  $60^\circ\text{C}$  for 2 h.

### Synthesis of Ag/AgCl@ZIF-8 photocatalyst

The overall preparation process of Ag/AgCl@ZIF-8 is illustrated in Scheme 1. In a typical procedure, 0.1 g of ZIF-8 powder was dispersed in 7 mL of  $53.7\text{ mmol L}^{-1}$  silver nitrate water:ethanol (v/v= 1:6) solution and stirred at room temperature for 3 h. And then, the mixture was injected dropwise to 49 mL of  $10.48\text{ mmol L}^{-1}$  sodium chloride water:ethanol (v/v= 1:6) solution within 20 min, the obtained solution was stirred at room temperature for 10 h. The color of the solution switched from white to light blue, suggesting the formation of Ag/AgCl@ZIF-8 heterostructures. The product was obtained by centrifugation and washed with deionized water for three times to remove excess sodium chloride. The light blue products were dried in a vacuum at  $60^\circ\text{C}$  for 2 h, and the obtained sample was denoted as 35wt.% Ag/AgCl@ZIF-8 (the mass ratios of AgCl to ZIF-8 were 35%). Similarly, the 20 wt.% Ag/AgCl@ZIF-8 and 50 wt.% Ag/AgCl@ZIF-8 were prepared according to the same procedure except 3.3 mL of  $53.7\text{ mmol L}^{-1}$  silver nitrate and 12.9 mL of  $53.7\text{ mmol L}^{-1}$  silver nitrate was added, respectively.



**Scheme 1** Schematic illustration of the synthetic processes of the Ag/AgCl@ZIF-8.

For comparison, Ag/AgCl photocatalysts were prepared by a precipitation method. 170 mg  $\text{AgNO}_3$  was dispersed in 25 mL deionized water under magnetic stirring at room temperature, and then the solution was injected dropwise to 25 mL  $40\text{ mmol L}^{-1}$  sodium chloride water solution within 20 min, the obtained solution was stirred at room temperature for 10 h. The color of the solution switched from white to pink, suggesting the formation of Ag/AgCl. The product was obtained by centrifugation and washed with deionized water for three times, and then dried in a vacuum at  $60^\circ\text{C}$  for 2 h.

### Photocatalytic degradation of RhB

The photocatalytic activities of Ag/AgCl@ZIF-8 nanocomposites were evaluated by the photodegradation of RhB. The photocatalytic reaction was conducted using a HSX-F/UV 300 Xe lamp (Beijing NBET Technology Co., Ltd) with a UV cutoff filter ( $\lambda \geq 420$  nm) in open air and at room temperature. In a typical process, 70 mg photocatalysts were added into 70 mL RhB aqueous solution ( $20 \text{ mg L}^{-1}$ ) in a beaker. Prior to light irradiation, the suspension was stirred for 1 h in the dark to ensure the adsorption/desorption equilibrium between the photocatalysts and the dyes. At the given time interval, about 3 mL suspension was withdrawn, centrifuged and filtered to remove the remained particles. The residual concentration of RhB was determined with a UV-vis spectrophotometer at 553 nm.

### Photoelectrochemical measurements

The photoelectric conversion properties of Ag/AgCl@ZIF-8 were investigated in a conventional three-electrode cell by using computer-controlled electrochemical workstation (CHI 660D). 50 mg catalysts was suspended in 2 mL nafion aqueous solution (1 wt.%), the mixtures were ultrasonically scattered for 15 min to form homogeneous solution. Then, 0.1 mL of the solution was dropped on the Indium tin oxide (ITO) glass ( $0.5 \times 4$  cm). After evaporation of the water in air, the catalyst was attached onto the surface of the ITO glass. The ITO glass, a Pt foil, saturated calomel electrode (SCE), and 0.1 mol  $\text{L}^{-1}$  sodium sulfate were used as the working electrode, the counter-electrode, the reference electrode, and the electrolyte, respectively. The current-time (I-t) curves were collected at 1 V vs SCE. A 300W Xe lamp was utilized as a light source, and a cutoff filter of 420nm was employed for the visible-light irradiation.

## Results and discussion

### Characterization of Ag/AgCl@ZIF-8 photocatalyst

The crystallographic structure of the as-prepared Ag/AgCl@ZIF-8 sample was examined by powder X-ray diffraction (PXRD). Figure 1 showed the XRD patterns of ZIF-8 and Ag/AgCl@ZIF-8. The sample of Ag/AgCl@ZIF-8 exhibited characteristic diffraction peaks of ZIF-8, which was in agreement with the reported crystal structure (space group I-43m)<sup>28</sup>. The XRD patterns of Ag/AgCl@ZIF-8 shown in Figure 1 were found to be comprised mainly of AgCl phase, which was characterized by the peaks located at  $2\theta$  values of  $27.8^\circ$ ,  $32.2^\circ$ ,  $48.3^\circ$ ,  $54.8^\circ$ ,  $57.4^\circ$ ,  $67.4^\circ$  and  $76.7^\circ$ , corresponding well to cubic phase AgCl according to JCPDS (31-1238). the peak at  $38.1^\circ$  (marked with “♦”) corresponding to the (111) crystal plane of Ag clearly represents the formation of Ag (JCPDS No. 04-0783), which could be ascribed to partial conversion of AgCl to elemental Ag through the reduction with sunlight during the process of preparation.

The morphology and particle size of the as-prepared ZIF-8 and Ag/AgCl@ZIF-8 samples were observed by SEM. The SEM image of ZIF-8 (Figure S1a, see ESI†) revealed the

original ZIF-8 particles to have a particle size of 100 nm and porous structure. As shown in Figure S1b, † the Ag/AgCl nanoparticles were well dispersed, indicating the well integrating between the Ag/AgCl nanoparticles and the ZIF-8. To further investigate the structural information, TEM was performed for the Ag/AgCl@ZIF-8, and a representative image was shown in Figure S1c. † The spacing between adjacent lattice fringes was 0.28 nm for AgCl and 0.24 nm for Ag, which is close to the d spacing of the (200) crystal plane of AgCl (JCPDS: 02-0848) and (111) plane of metallic Ag (JCPDS: 04-0783).

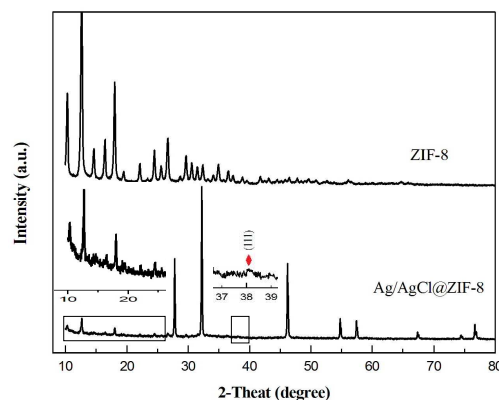


**Figure 1.** XRD pattern of ZIF-8 and Ag/AgCl@ZIF-8

Specific surface area and porous structure of ZIF-8 and Ag/AgCl@ZIF-8 were determined by  $\text{N}_2$  adsorption-desorption isotherms at 77 K (Figure S2, †). The BET surface area and total pore volume of Ag/AgCl@ZIF-8 were calculated to be  $483.4 \text{ m}^2 \cdot \text{g}^{-1}$  and  $0.32 \text{ cm}^3 \cdot \text{g}^{-1}$ , respectively, which is lower than that of ZIF-8 ( $1319.4 \text{ m}^2 \cdot \text{g}^{-1}$  and  $1.03 \text{ cm}^3 \cdot \text{g}^{-1}$ ). The great decrease in the amount of  $\text{N}_2$  adsorption and the pore volume of Ag/AgCl@ZIF-8 indicated that the pores of the ZIF-8 were occupied by the highly dispersed Ag/AgCl nanoparticles.

The UV-visible diffuse reflectance spectra of Ag/AgCl@ZIF-8, Ag/AgCl and ZIF-8 were shown in Figure 2. Compared with Ag/AgCl and ZIF-8, the Ag/AgCl@ZIF-8 exhibited a broader and stronger absorption in the visible-light region, which can be attributed to the surface plasmon resonance of silver nanoparticles and the unique hetero-junction structure of Ag/AgCl@ZIF-8. After integrated with ZIF-8, Ag/AgCl@ZIF-8 has a large number of different shapes and diameter, the surrounding environment of Ag/AgCl is also changed, so that the plasmon oscillations cover a wide range of frequencies. Hence Ag/AgCl@ZIF-8 can absorb a wide range of visible light and lead to the production of more electron-hole pairs under the visible light irradiation, which subsequently resulted in a higher photocatalytic activity.

XPS analysis confirms the presence of Ag, Cl, Zn, C and N in the Ag/AgCl@ZIF-8 hybrid composites (Figure S3, †). Two specific peaks of Ag 3d located at ca. 368 and 374 eV could be attributed to the Ag  $3d_{5/2}$  and Ag  $3d_{3/2}$  binding energies (Figure S3a, †), respectively, and these bands display nearly 0.5 eV shift to higher binding energy compared with the Ag  $3d_{3/2}$  and

Ag  $3d_{5/2}$  in AgCl,<sup>29</sup> which may be partially due to the interaction among the Ag, AgCl and ZIF-8. The deconvolution of these two bands gives out peaks at 374.3, 373.9 eV and 368.6, 367.9 eV, respectively. The peaks at 374.3 and 368.6 eV could be attributed to the metallic Ag<sup>0</sup>, while the peaks at 373.9 and 367.9 eV could be attributed to the Ag<sup>+</sup> of AgCl. These results confirm the existence of metallic Ag<sup>0</sup> in our Ag/AgCl@ZIF-8 hybrid nanocomposites.

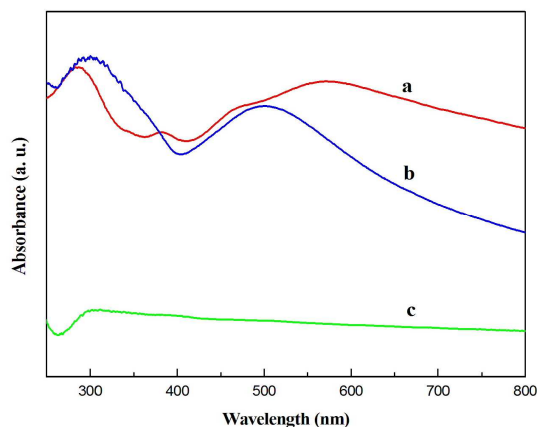


**Figure 2.** UV-vis DRS spectra of (a) Ag/AgCl@ZIF-8, (b) Ag/AgCl, and (c) ZIF-8.

### Photocatalytic degradation of RhB

The UV-vis spectra of RhB aqueous solution in the presence of Ag/AgCl@ZIF-8 nanocomposites under visible-light irradiation ( $\lambda \geq 420$  nm) at room temperature for different durations are shown in Figure 3. The main absorption peak at 553 nm corresponding to the RhB molecule decreases rapidly with extension of the exposure time, and completely disappears after irradiation for about 16 min.

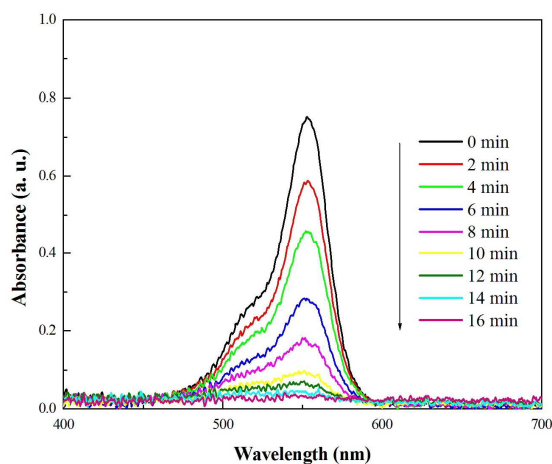


**Figure 3.** The absorption variation of RhB dye over as-synthesized 35 wt% Ag/AgCl@ZIF-8 at different irradiation time.

The photocatalytic activities of 35 wt.% Ag/AgCl@ZIF-8 for the photo-degradation of RhB under visible light irradiation were compared with that of the other obtained photocatalyst. As shown in Figure 4a, it is clear that the degradation of RhB by

using commercial TiO<sub>2</sub> particles P25 as visible-light response photocatalyst could be neglected. The Ag/AgCl and the ZIF-8 could degrade RhB by 48% and 46%, respectively, under visible light irradiation for 16 min (Figure 4b,4c), which is consist with the results reported in the reference.<sup>20</sup> To our delight, the integration of Ag/AgCl with ZIF-8 could significantly enhance the photocatalytic activity of the composite (Figure 4d,4e,4f). Moreover, the photocatalytic efficiency of the 35wt.% Ag/AgCl@ZIF-8 (Figure 4e) was much higher than that of 20wt.% Ag/AgCl@ZIF-8 and similar to that of 50wt.% Ag/AgCl@ZIF-8. When the amount of Ag/AgCl was higher than 35wt.%, the photoactivity of the Ag/AgCl@ZIF-8 sample no longer increased, which probably because the larger Ag/AgCl nanoparticle size lead to the anchored force between the substrate and Ag/AgCl becomes weaker, which could destruct the hetero-junction structure<sup>30</sup>. Apparently, the unique hetero-junction structure of 35wt.% Ag/AgCl@ZIF-8 greatly enhanced its photocatalytic activity.

As shown in Figure 4e, the 35 wt.% Ag/AgCl@ZIF-8 could degrade RhB by 98% under visible light irradiation for 16 min. Compared with the Ag/AgCl photocatalyst, the photocatalytic degradation efficiency of 35 wt.% Ag/AgCl@ZIF-8 for RhB was enhanced about 50%. It should be noted that the dosage of Ag/AgCl in 35 wt.% Ag/AgCl@ZIF-8 was only about one-third of that in Ag/AgCl catalyst. The high activity of 35 wt.% Ag/AgCl@ZIF-8 could be attributed to the synergic effect between ZIF-8 and Ag/AgCl, which might include the high specific surface areas of ZIF-8, the well dispersion of Ag/AgCl on ZIF-8 and enhanced optical property. MOF usually exhibits a higher adsorption capacity for the organic molecules, which is also beneficial for the enhancement of the photocatalytic activity of Ag/AgCl@ZIF-8 composite.

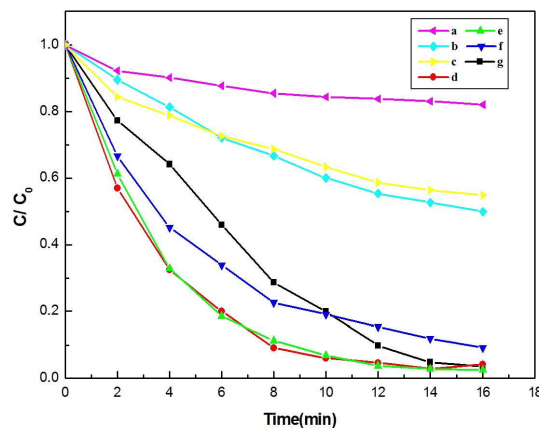


**Figure 4.** The photodegradation of RhB with different photocatalyst. (a) P25, (b) Ag/AgCl, (c) ZIF-8, (d) 50 wt.% Ag/AgCl@ZIF-8, (e) 35 wt.% Ag/AgCl@ZIF-8, and (f) 20 wt.% Ag/AgCl@ZIF-8 under visible light irradiation, (g) 35 wt.% Ag/AgCl@ZIF-8 under sunlight irradiation. 70 mg photocatalysts were added into 70 mL RhB aqueous solution ( $20 \text{ mg L}^{-1}$ ).

The photoactivity of 35 wt.% Ag/AgCl@ZIF-8 and the mixture of the Ag/AgCl and ZIF-8 was compared under the

same conditions. The results were shown in Figure S4. † It can be seen that the Ag/AgCl@ZIF-8 shows much higher photoactivity than the mixture of Ag/AgCl and ZIF-8, which demonstrated that the synergetic effect between the Ag/AgCl and ZIF-8, and the unique hetero-junction structure of Ag/AgCl@ZIF-8 are responsible for the enhancement of the photocatalytic activity.

On the basis of the obtained results, the photocatalytic activity of 35 wt.% Ag/AgCl@ZIF-8 for the decomposition of RhB by directly harvesting solar energy was also investigated. As can be seen from Figure 4g, 98% of RhB was degraded after 16 min under solar radiation. The high degradation efficiency obtained under solar radiation points out the potential of directly harvesting solar energy to overcome the energy barriers in solving environmental issues such as air and water pollution.

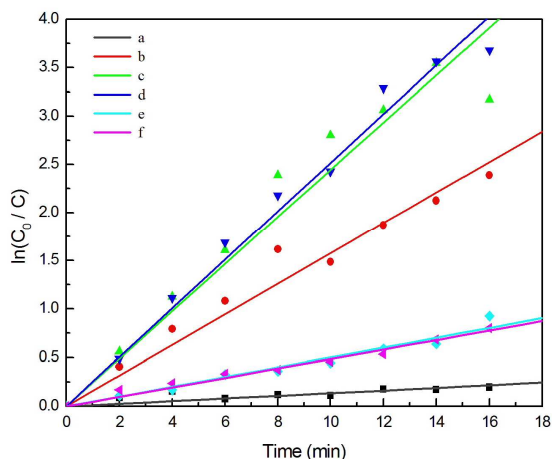


**Figure 5.** The first-order kinetics of RhB degradation in the presence different samples (a) P25 (b) 20 wt.% Ag/AgCl@ZIF-8 (c) 50 wt.% Ag/AgCl@ZIF-8 (d) 35 wt.% Ag/AgCl@ZIF-8 (e) Ag/AgCl (f) ZIF-8. 70 mg photocatalysts were added into 70 mL RhB ( $20 \text{ mg L}^{-1}$ ) aqueous solution.

The corresponding  $\ln(C_0/C)$  plot has a good linearity (Figure 5), indicating that the visible light-driven photodegradation of RhB in the presence of Ag/AgCl@ZIF-8 follows the first-order kinetics. The degradation rate constants of different photocatalysts are shown in Figure 6. The degradation rate constant of 35 wt.% Ag/AgCl@ZIF-8 is as high as 18.54 times to that of commercial P25.

Currently, it was widely accepted that the separation efficiency of electrons and holes played a vital role in the photocatalytic reaction: the higher the photocurrent was, the better the electron and hole separation efficiency would be, and thus the higher the photocatalytic activity would be.<sup>30, 31</sup> The photoelectric conversion properties over Ag/AgCl@ZIF-8 deposited on the Indium tin oxide (ITO) glass have been investigated in detail. As shown in Figure 7, the Ag/AgCl@ZIF-8 hybrid materials showed a noticeable photocurrent under visible light irradiation. It was also found that the Ag/AgCl@ZIF-8 hybrid materials had the stable photocurrent, which indicated that the hybrid materials had lower rate to recombine electrons and holes.<sup>30, 31</sup>

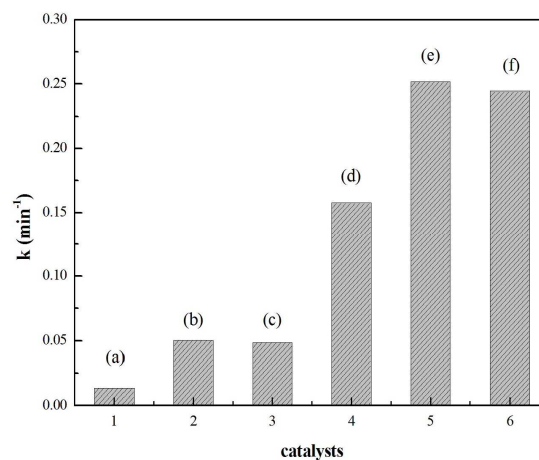


**Figure 6.** The degradation rate constant of RhB with different samples: (a) P25 (b) Ag/AgCl (c) pure ZIF-8 (d) 20 wt.% Ag/AgCl@ZIF-8 (e) 35 wt.% Ag/AgCl@ZIF-8 (f) 50 wt.% Ag/AgCl@ZIF-8.

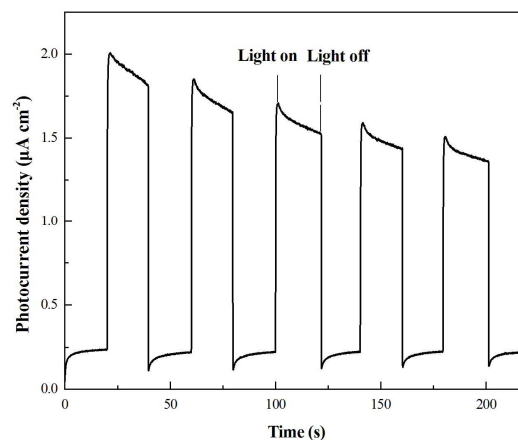


**Figure 7.** Photoelectric conversion performances of 35 wt.% Ag/AgCl@ZIF-8 in  $0.1 \text{ mol L}^{-1} \text{ Na}_2\text{SO}_4$  aqueous solution under 300 W Xe lamp irradiation.

On the basis of the obtained results in the present work, a possible photocatalytic mechanism was proposed to clarify the higher photocatalytic activity of Ag/AgCl@ZIF-8 heterostructures than Ag/AgCl and ZIF-8. Ag nanoparticles possess a low Fermi level, which can serve as a good electron acceptor for facilitating quick electron transfer from AgCl microsphere under visible-light irradiation. Therefore, the photo excited electrons can be rapidly transferred to Ag nanoparticles and then transferred to ZIF-8,<sup>21</sup> while the photo induced holes still located on the AgCl microsphere, which promoted the effective separation of photo excited electron-hole pairs and decreased the probability of electron-hole recombination. The photo excited electrons could be transferred to molecular oxygen, which was adsorbed on the surface of the catalyst to generate superoxide radical ( $\text{O}_2^{\cdot-}$ ).<sup>32</sup> The  $\text{O}_2^{\cdot-}$  could induce the degradation of RhB. The high concentration of holes on AgCl microsphere could combine with  $\text{H}_2\text{O}$  molecules adsorbed on the surface of the catalyst to produce  $\cdot\text{OH}$  radicals, which were thought to induce the degradation of RhB in the reaction.<sup>33</sup> On

the other hand, the photo catalytic process is known to be related to the adsorption and desorption of molecules onto the surface of catalysts. <sup>34</sup> ZIF-8 in the composite could adsorb the organic compounds from the aqueous solution and transfer it to the photocatalyst surface. As a result, the Ag/AgCl@ZIF-8 hybrid microspheres exhibit excellent photocatalytic activity for degradation of RhB under visible-light irradiation.

It was worth pointing out that the stability of the photocatalyst was crucial for the practical application. The stability test of the Ag/AgCl@ZIF-8 hybrid material was conducted by performing the RhB bleaching reactions repeatedly for six times, as shown in Figure 8. The photocatalytic efficiency decreased slightly after six times due to the loss of catalyst in the recycling process, and the catalyst still exhibited high activity after six successive cycles under the visible light irradiation. These results indicated that Ag/AgCl@ZIF-8 hybrid material is an effective and reusable visible-light response photocatalyst.

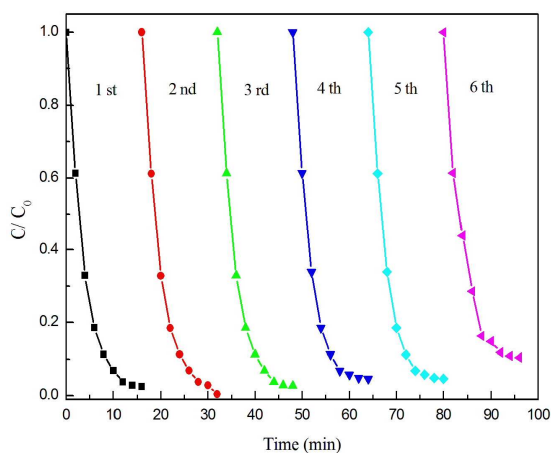


**Figure 8.** The cycling runs of the degradation of RhB (20 mg/L<sup>-1</sup>) over 35 wt.% Ag/AgCl@ZIF-8 catalyst.

## Conclusions

In this report, a visible-light-response photocatalyst 35 wt.% Ag/AgCl@ZIF-8 was facilely synthesized for the first time by integrating a plasmonic photocatalyst with metal-organic framework material. The Ag/AgCl deposited on the surface of the ZIF-8 could transfer the electron generated from Ag/AgCl to ZIF-8 and suppress the electron-hole recombination of it. At the same time, the ZIF-8 could adsorb RhB effectively and further enhance photoactivity of Ag/AgCl. The results demonstrated that the as-prepared Ag/AgCl@ZIF-8 photocatalysts exhibit high activity and durability towards decomposition of RhB under visible light irradiation or sunlight, which can be attributed to the synergic effect between ZIF-8 and Ag/AgCl, and the unique hetero-junction structure of Ag/AgCl@ZIF-8. The results revealed that the 35 wt.% Ag/AgCl@ZIF-8 is an efficient, low-cost, recyclable visible-light-response photocatalysts. These findings in the current work could provide a general guiding line for designing novel visible-light-response photocatalyst to harvest solar energy,

which would be found promising applications in environmental purification and energy conversion.

## Acknowledgements

This work was financially supported by the National Natural Science Foundation of China (no. 31171698, 31471643), the Innovation Research Program of Department of Education of Hebei for Hebei Provincial Universities (LJRC009), Natural Science Foundation of Hebei Province (no. B2011204051) and the Natural Science Foundation of Agricultural University of Hebei (LG201404).

## Notes and references

College of Sciences  
Agricultural University of Hebei  
Baoding 071001, Hebei Province, P. R. China  
Fax: (+86)312-7528292  
E-mail: chunwang69@126.com  
Electronic Supplementary Information (ESI) available: Characterization data of all products. See DOI: 10.1039/b000000x/

- 1 C. Chen, W. Ma and J. Zhao, *Chem. Soc. Rev.*, 2010, **39**, 4206.
- 2 T. Zhang and W. Lin, *Chem. Soc. Rev.*, 2014, **43**, 5982.
- 3 A. Aijaz, T. Akita, H. Yang and Q. Xu, *Chem. Commun.*, 2014, **50**, 6498.
- 4 X. Gu, Z. H. Lu and Q. Xu, *Chem. Commun.*, 2010, **46**, 7400.
- 5 Y. X. Tan, F. Wang, Y. Kang and J. Zhang, *Chem. Commun.*, 2011, **47**, 770.
- 6 Y. S. Bae, O. K. Farha, A. M. Spokoyny, C. A. Mirkin, J. T. Hupp and R. Q. Snurr, *Chem. Commun.*, 2008, 4135.
- 7 Y. Huang, T. Ma, P. Huang, D. Wu, Z. Lin and R. Cao, *ChemCatChem*, 2013, **5**, 1877.
- 8 L. Zhang, Z. Su, F. Jiang, Y. Zhou, W. Xu and M. Hong, *Tetrahedron*, 2013, **69**, 9237.
- 9 M. Zhang, J. Guan, B. Zhang, D. Su, C. T. Williams and C. Liang, *Catal. Lett.*, 2012, **142**, 313.
- 10 Y. Zhao, M. Padmanabhan, Q. Gong, N. Tsumori, Q. Xu and J. Li, *Chem. Commun.*, 2011, **47**, 6377.
- 11 W. W. Zhan, Q. Kuang, J. Z. Zhou, X. J. Kong, Z. X. Xie and L. S. Zheng, *J. Am. Chem. Soc.*, 2013, **135**, 1926.
- 12 P. Su, H. Xiao, J. Zhao, Y. Yao, Z. Shao, C. Li and Q. Yang, *Chem. Sci.*, 2013, **4**, 2941.
- 13 A. J. Amali, J. K. Sun and Q. Xu, *Chem. Commun.*, 2014, **50**, 1519.
- 14 K. T. Butler, C. H. Hendon and A. Walsh, *J. Am. Chem. Soc.*, 2014, **136**, 2703.
- 15 F.-X. Qin, S.-Y. Jia, Y. Liu, X. Han, H.-T. Ren, W.-W. Zhang, J.-W. Hou and S.-H. Wu, *Mater. Lett.*, 2013, **101**, 93.
- 16 F. X. L. Xamena, A. Corma and H. Garcia, *J. Phys. Chem. C*, 2007, **111**, 80.
- 17 J. J. Du, Y. P. Yuan, J. X. Sun, F. M. Peng, X. Jiang, L. G. Qiu, A. J. Xie, Y. H. Shen and J. F. Zhu, *J. Hazard. Mater.*, 2011, **190**, 945.
- 18 W. T. Xu, L. Ma, F. Ke, F. M. Peng, G. S. Xu, Y. H. Shen, J. F. Zhu, L. G. Qiu and Y. P. Yuan, *Dalton Trans.*, 2014, **43**, 3792.

## Journal Name

- 19 J. Gao, J. Miao, P. Z. Li, W. Y. Teng, L. Yang, Y. Zhao, B. Liu and Q. Zhang, *Chem. Commun.*, 2014, **50**, 3786.
- 20 L. H. Wee, N. Janssens, S. P. Sree, C. Wiktor, E. Gobechiya, R. A. Fischer, C. E. Kirschhock and J. A. Martens, *Nanoscale*, 2014, **6**, 2056.
- 21 R. Li, J. Hu, M. Deng, H. Wang, X. Wang, Y. Hu, H. L. Jiang, J. Jiang, Q. Zhang, Y. Xie and Y. Xiong, *Adv Mater*, 2014, **26**, 4783.
- 22 M.S Zhu, P. L. Chen. and M. H. Liu, *Progress Chem.*, 2013, **25**, 209.
- 23 S. T. Gao, N. S. Shang, C. Feng, C. Wang and Z. Wang, *RSC Adv.*, 2014, 39242.
- 24 S. R. Venna and M. A. Carreon, *J. Am. Chem. Soc.*, 2010, **132**, 76.
- 25 G. Lu, O. K. Farha, W. Zhang, F. Huo and J. T. Hupp, *Adv. Mater.*, 2012, **24**, 3970.
- 26 C. Chizallet, S. Lazare, D. BazerBachi, F. Bonnier, V. Lecocq, E. Soyer, A. A. Quoineaud and N. Bats, *J. Am. Chem. Soc.*, 2010, **132**, 12365.
- 27 J. Cravillon, S. Münzer, S. J. Lohmeier, A. Feldhoff, K. Huber and M. Wiebcke, *Chem. Mater.*, 2009, **21**, 1410.
- 28 K. S. Park, Z. Ni, A. P. Cote, J. Y. Choi, R. Huang, F. J. Uribe-Romo, H. K. Chae, M. O'Keeffe and O. M. Yaghi, *PNAS*, 2006, **103**, 10186.
- 29 M.S Zhu, P. L. Chen. and M. H. Liu, *ACS Nano*, 2011, **5**, 4529.
- 30 H. Xu, J. Yan, Y. Xu, Y. Song, H. Li, J. Xia, C. Huang and H. Wan, *Appl. Catal. B: Environ.*, 2013, **129**, 182.
- 31 J. Jiang, X. Zhang, P. Sun and L. Zhang, *J. Phys. Chem. C*, 2011, **115**, 20555.
- 32 P. Wang, B. Huang, X. Qin, X. Zhang, Y. Dai, J. Wei and M. H. Whangbo, *Angew Chem. Int. Ed*, 2008, **47**, 7931.
- 33 W. Cui, H. Wang, L. Liu, Y. Liang and J. G. McEvoy, *Applied Surface Sci.*, 2013, **283**, 820.
- 34 Y. W. Wang and L. Zhang, *J. Phys. Chem. C*, 2009, **113**, 9210.